J Electroceram (2009) 22:91–97
DOI 10.1007/s10832-008-9421-6

Thermoelectric $Ca_3Co_4O_9$ ceramics consolidated by Spark Plasma sintering

J. G. Noudem · M. Prevel · A. Veres · D. Chateigner · J. Galy

Received: 29 March 2007 / Accepted: 10 January 2008 / Published online: 30 January 2008

Abstract Hole-doped $Ca_3Co_4O_9$ (Co349) ceramics were prepared using solid-state reaction. Two processing strategies have been used to produce the thermoelectric oxide ceramics, Conventional and Spark Plasma (SPS) Sintering to control the grains consolidation, texturation and sample densification. Thermoelectric properties were measured and the influence of the processing conditions on the properties was evidenced. SPS favours shorter elaboration times and produces samples with larger thermoelectric properties due to better densification and alignment. The effect of the free deformation and texturation using the SPS technique is discussed. Seebeck coefficient values of 180 μV/K at 873 K are obtained.

Keywords Thermoelectric materials · Ceramics · Oxides · P-type · Texture

1 Introduction

Since the discovery of the thermoelectricity (TE) in the $NaCo_2O_4$ phase [1], intensive research has been devoted to discover new oxide materials [2–9], in order to improve potential TE properties [5, 9–12] and/or to develop TE modules for power generation [13–16].

J. G. Noudem (✉) · M. Prevel · A. Veres · D. Chateigner
CRISMAT laboratory, CNRS UMR 6508, ENSICAEN,
Université de Caen Basse-Normandie,
6 bd du Marechal Juin,
14050 Caen, France
e-mail: jacques.noudem@ensicaen.fr

J. Galy
CEMES, CNRS,
29, rue Jeanne-Marvig,
31055 Toulouse, France

Most of the used elaboration processes for $Ca_3Co_4O_9$ (Co349) are based on classical solid-state reaction relying basically on conventional sintering [17]. Single crystal composite templating [18], reactive template grain growth [19], hot pressing [20], sinter-forging [11, 21], and magnetic field [22] are also used to densify and/or to induce an orientation between grains. In addition, the novel Spark Plasma Sintering (SPS) technique has been developed and commonly used nowadays to prepare various materials [23–27]. The SPS is a unique sintering method combining mechanical pressure and an electric energy in a pulse shape as the heat source for sintering [28]. The mixed raw material is directly poured into the die assembly made of electrically conductive materials without any additive or binder and pressed uniaxially by punches while the DC current is supplied in the die assembly holding the powder compact. One of the main advantages of the SPS technique has been demonstrated to be the rapid densification of various materials in a very short time (a few minutes) with respect to the Conventional Sintering (CS) method.

In this study, we report the free deformation and texturation of pre-sintered lamellar $Ca_3Co_4O_9$ (Co349) ceramic powders using the SPS technique.

The purpose of this paper is to describe the process and present first texturation and TE results. Quantitative texture analysis of the bulk ceramic material is investigated together with microstructure using X-ray diffraction (XRD), and are correlated to the thermoelectric properties.

2 Experimental procedure

The ceramic powder of $Ca_3Co_4O_9$ was prepared using classical solid-state reaction. A mixture of commercially available $CaCO_3$ (calcite) and Co_2O_3 precursors was

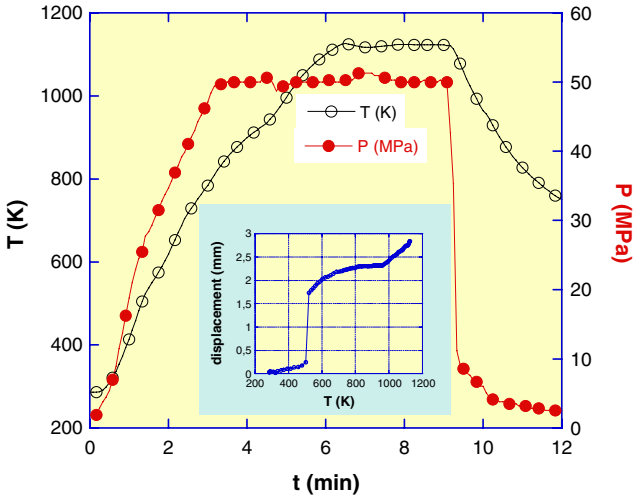

Fig. 1 Temperature and applied pressure versus sintering time during SPS elaboration. *Insert*, temperature dependence of sample's dimension displacement

calcined twice in air at 1173 K during 24 h with an intermediate grinding. The mixture was cold pressed unidirectionally at 60 MPa into cylindrical pellets with a diameter of 13 mm. The preformed pellets were conventionally sintered (CS) at 1193 K, 24 h and placed at the centre of the graphite die with a diameter of 20 mm with the aim to ensure the free deformation and texturation of the sample. The final processing was carried out using the Spark Plasma Sintering system (Dr. Sinter SPS 2080, Sumitomo Coal Mining Co., Ltd., Japan). The pulsed electric current (2000 A, 4 V) was passed through the sample under vacuum (10^{-3} bar) and a uniaxial pressure of 50 MPa was applied. During the experiment, the temperature, applied pressure and displacement or shrinkage of the sample was recorded (Fig. 1). Samples were heated for comparison at two different temperatures, 1023 and 1123 K, while a load of 15 kN (50 MPa) was applied during 2 min. The as-prepared sample was polished to remove the graphite foil used during processing, then heated at 1073 K for 6 h under oxygen to ensure the desired stoichiometry.

Diffraction experiments were first carried out using a Philips θ–2θ diffractometer using the monochromatic Cu-Kα radiation. Then quantitative texture analysis was measured on a Huber 4-circle diffractometer equipped with a curved position sensitive detector (CPS120 from INEL) [29], on the surface perpendicular to the applied uniaxial pressure. Since uniaxial pressure produces axially symmetric textures, only one scan in tilt angle (χ) was operated, during which the whole 2θ diagrams were collected with a resolution of $\Delta 2\theta = 0.03°$, up to $\chi = 60°$ with angular increments $\Delta\chi = 5°$. Diagrams were exploited within the combined analysis approach [30] as implemented in the materials analysis using diffraction program package [31] to analyse texture from the whole patterns, including crystal structure and sample coherent domain sizes. Briefly, in this approach, the Rietveld method [32] for structure determination is combined with the Williams–Imhof–Matthies–Vinel formalism [33] for the calculation of the Orientation Distribution Function (ODF). The ODF is then used to calculate the complete pole figures, otherwise obtained incompletely due to X-ray defocusing [34]. The instrument was calibrated and its signal deconvoluted from sample contribution in the diffraction profiles for all scanned positions of the sample, by measuring the SRM660 LaB_6 standard from the National Institute of Standards and Technology. Due to the modulated structure of Co349, the supercell structure with b~8b1~13b2 has been used for the refinement.

Samples for microstructural analysis were prepared by fracturing the samples parallel to the stress applied during processing and examined using a *Philips XL 30 FEG*, scanning electron microscope, in backscattering mode.

Bar-shaped samples for physical characterization with dimensions of 10 mm long and 2×2 mm^2 cross section were cut from the heat-treated samples using a low speed diamond saw (Struers, Champigny sur Marne, France). The thermoelectric properties were measured by the dc four-probe method using the Seebeck coefficient and electrical resistivity measuring system ZEM-3 (ULVAC-RIKO, Inc., Japan) from room temperature to 873 K.

3 Results and discussion

The $Ca_3Co_4O_9$ phase formation was assessed using XRD measurements (Fig. 2). The diagrams show a good crystallisation of the phase with sharp peaks. The measure-

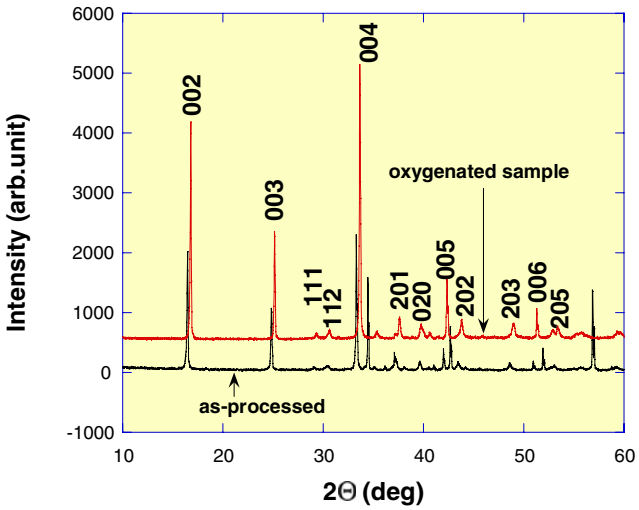

Fig. 2 XRD patterns of the SPS sample measured on a surface perpendicular to the uniaxial pressure direction, for the as-processed (*top/red*) and oxygen annealed (*bottom/black*) samples

ments were performed at room temperature on the polished surface of the bulk samples. The as-processed sample shows that the Co349 phase is not completely formed probably due to low oxygen content, and coherently to a slight shift in peak positions compared to the fully oxygenated Co349. After oxygen annealing all XRD peaks can be indexed and are at the theoretical positions for Co349. The XRD peaks corresponding to {00ℓ} planes are prominent, pointing out for a strong grain alignment in the polycrystalline sample due to the uniaxial pressure. These classical θ–2θ diffraction patterns are very similar to previously reported [3, 27] data for oriented $Ca_3Co_4O_9$, with platelet grains aligned perpendicularly to the pressure axis. However, they do not reveal the orientation distribution of the {00ℓ} planes out of the normal to the sample.

A quantitative texture analysis was then carried out using the combined approach of full patterns simulation. The whole χ-scan dataset (Fig. 3(a)) exemplifies the typical data simulation obtained on that kind of samples. The prominent 00ℓ lines at χ=0, progressively vanish as c-axis increases, as a sign of the orientation distribution of crystallites. This decrease is made more visible on a 2D diagram (Fig. 3(a)). The refined values of the unit-cell resulting from the combined analysis are a=4.8424(4)Å, b=36.493(3)Å, c=10.8446(3) Å and β=98.000(6)° for the SPS sample elaborated at 1123 K, and a=4.8361(7)Å, b=36.450(5)Å, c=10.8333(3) Å and β=98.030(8)° for the SPS sample elaborated at 1023 K. These values are perfectly in accordance with the supercell parameters [3, 11] of the Co349 phase. The reliability factors for the Rietveld refinement of the whole dataset are Rw=2.1%, Rexp=1.05% and a Goodness of Fit of χ^2=4.07 for SPS-1123 K, and 2.42%, 1.06%, 5.15 for SPS-1023 K. The pole figures reconstructed from the ODF (Fig. 3(a)) clearly demonstrate the {00ℓ} alignment of the crystallites in the sample, within a reliability factor of Rw=1.71% and 1.86% for SPS-1123 K and SPS-1023 K respectively. The maximum of the distribution near 4.9 m.r.d. on the {001} pole figure for both samples is comparable to the average orientations observed so far in Co349 ceramics [18, 19, 21, 35]. The minimum of density is nearly 0, indicating that no other orientation component is present in the samples.

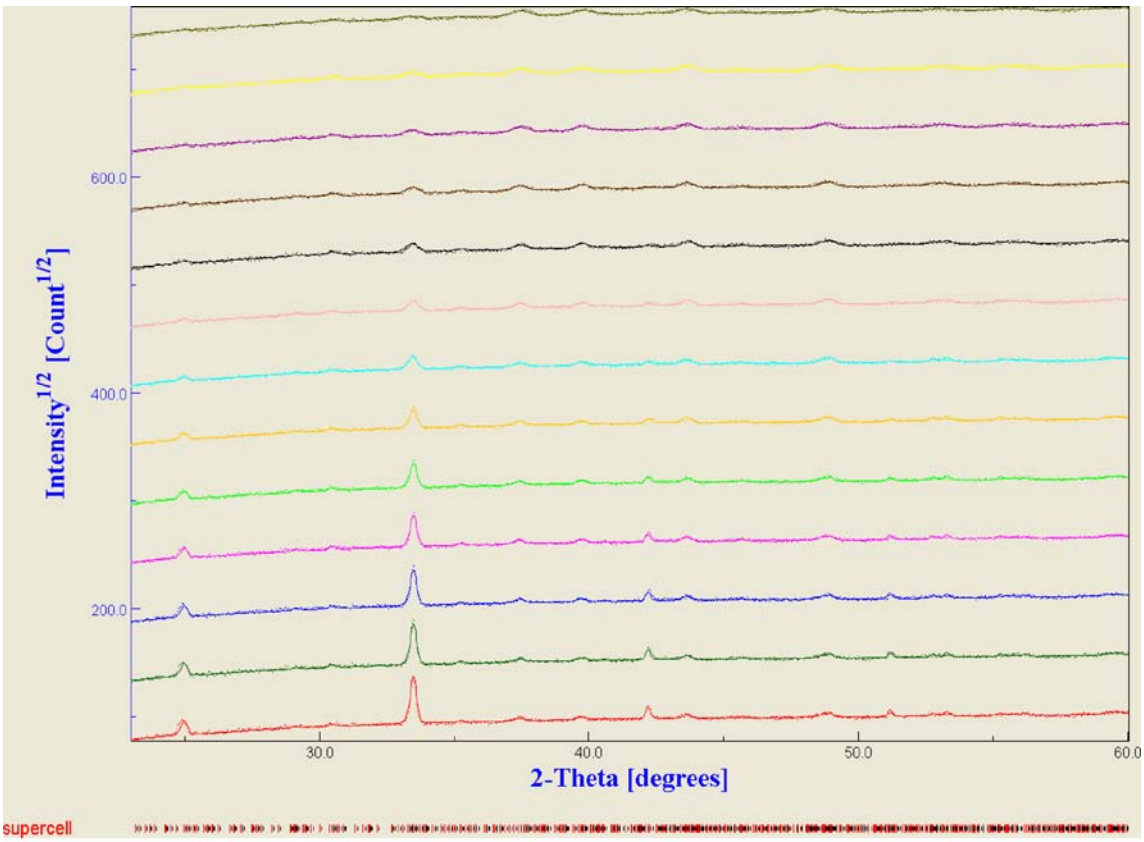

Fig. 3 **(a)** Experimental (dots) and simulated (*line*) χ-scan data obtained using the combined analysis on the SPS Co349 sample. Note the intensity is represented on a square root scale to respect statistical errors for all the 2θ range. *Bottom diagram*, χ=0°; *top diagram*, χ=60° increments in χ were 5°. **(b)** 2D representation of the previous diagrams, with experimental (*bottom*) and simulated (*top*) datasets. **(c)** {010}, {001} and {100} pole figures of Co349 in the SPS/1123K (*top*) and SPS/1023K (*bottom*) samples. Linear density scale, equal area projection. The pressure axis is the centre of the pole figures

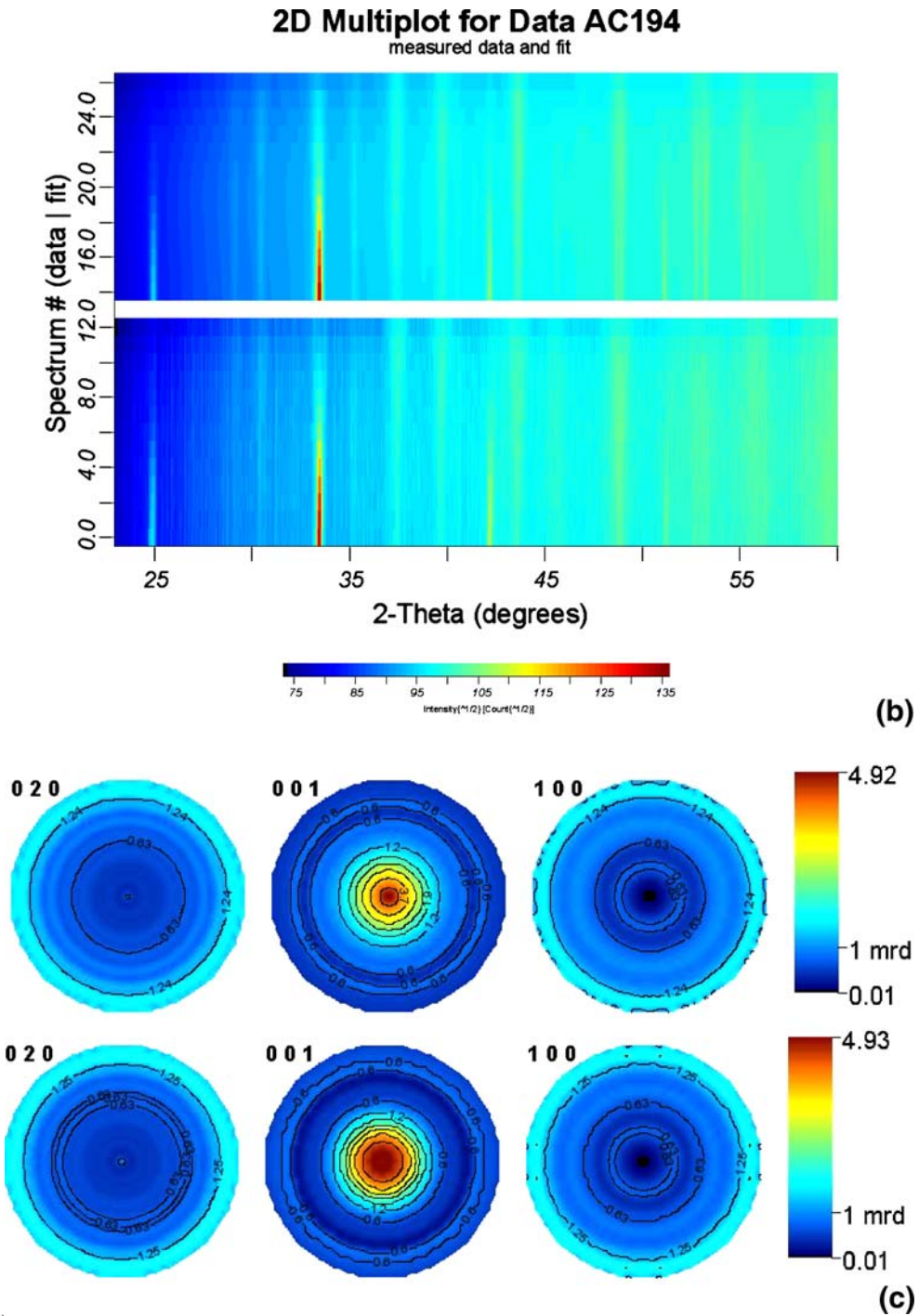

Fig. 3 (continued)

Figure 4 shows the scanning electron microscopic (SEM) images from the fractured cross sections of the reference sample processed by CS, and of the SPS processed. The CS specimen contains more pores than the SPS specimen, and the platelets in the SPS specimen were well aligned with the average c-axis parallel to the uniaxial pressure applied during the hot-deformation. The Co349 sample classically sintered at 1193 K (Fig. 4, bottom-left insert) exhibits underdeveloped grains with a porous microstructure compared to the already well compact and crystallised grains observed for SPS elaboration at 1023 K (Fig. 4, top-right insert). This is a neat advantage for SPS to produce denser microstructure at lower temperature than for CS process. At an intermediate temperature of 1123 K (Fig. 4), the SPS sample shows very well crystallised grains with well oriented and developed crystal faces. The bulk

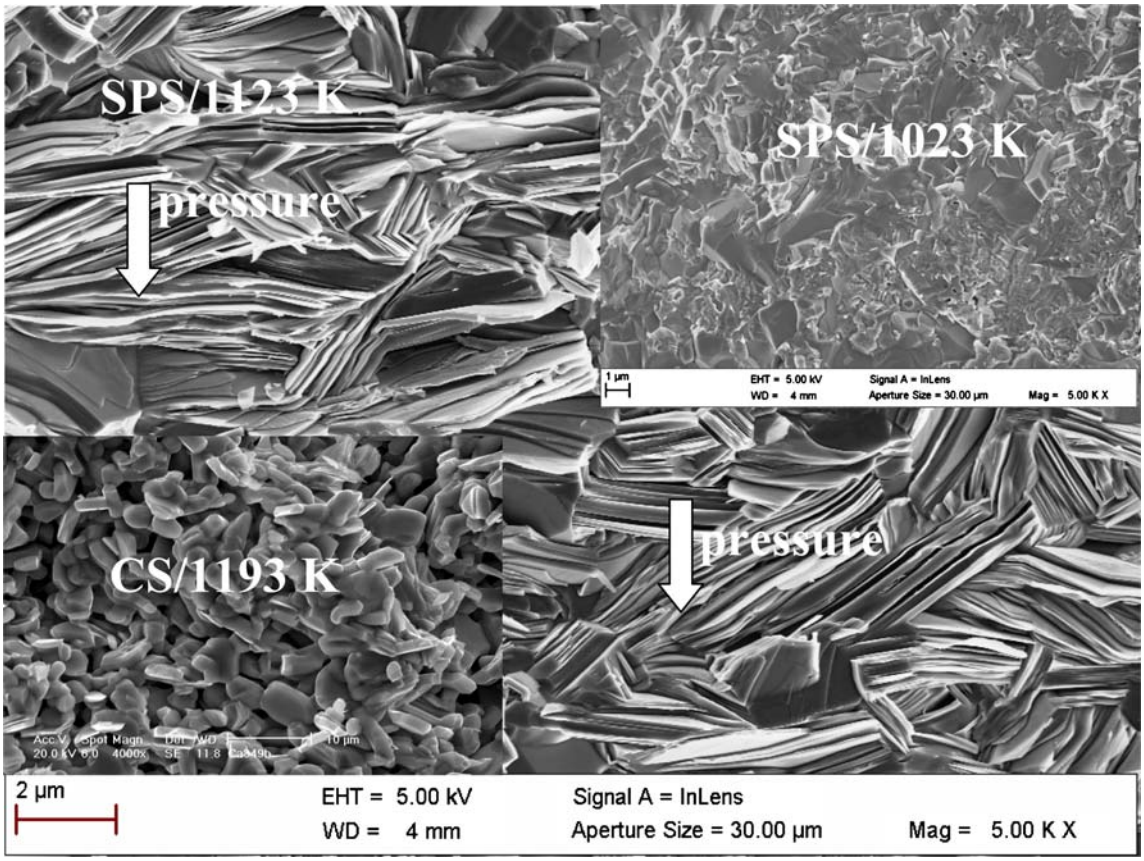

Fig. 4 Backscattering SEM micrographs observed at a fracture section of SPS, 1123K. *Top-right insert* is an SPS sample elaborated at 1023K, *bottom-left insert* corresponds to a conventionally sintered sample at 1193 K, 24 h

density of the samples are 3.1 (CS, 1193 K) 4.45 (SPS, 1023 K) and 4.57 g/cm^3 (SPS, 1123 K) corresponding to 57%, 95% and 98% respectively of the theoretical density [3]. The densification of the SPS sample is correlated to the temperature dependence of the sample displacement or shrinkage (Fig. 1, insert) during processing. It could be seen that the sample densified quickly between 473–573 and 923–1123 K. At 1123 K densification is still not completed, further shrinkage being available when temperature increases further.

The temperature dependence of the resistivity (ρ) and the thermoelectric power (S) from 325 to 873 K were investigated (Fig. 5). The standard deviation is ±0.5 for electrical and power factor experimental data. The resistivity slope in this temperature range exhibits a different behaviour between CS and SPS samples. While the behaviour of the CS sample is clearly metallic above 600 K, and roughly semiconducting-like below, the SPS samples show an opposite slope in this temperature range. Since the CS sample is porous dense, its behaviour below 600 K is strongly linked to porosity or intergranular medium, not relevant of the phase behaviour. When grain connections establish with sintering, the natural metallic behaviour is exhibited. The two SPS samples show the same resistivity behaviour, however with resistivity values of 6 and 8 mΩ.cm measured for the SPS/1023 K and SPS/1123 K samples respectively. These values are five times lower than the resistivity of the CS sample for which 30 and 35 mΩ.cm were measured at room temperature and at

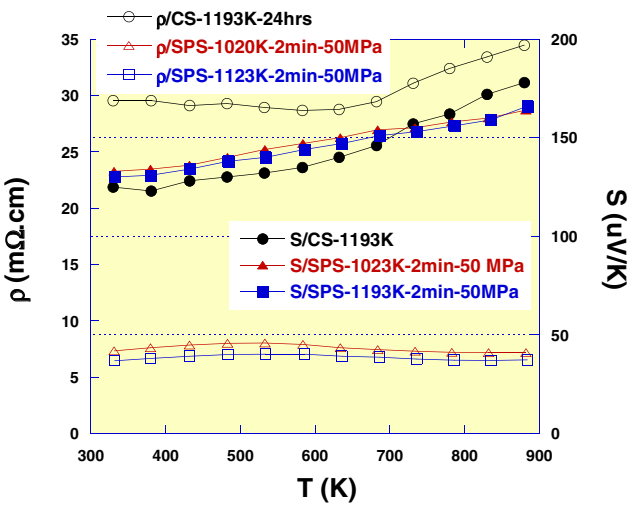

Fig. 5 Temperature dependence of electrical resistivity (*filled symbols*) and Seebeck coefficient (*open symbols*)

873 K respectively. This clearly shows that the resistivity has been decreased by increasing the sample density and inducing the platelet alignment using the SPS technique. The slightly larger resistivity of the SPS sample elaborated at 1023 K can be due to its slightly lower density. However one cannot exclude a priori an effect of its larger crystallite distribution, as seen in the broader centre of its {001} pole figure compared to SPS-1123K.

The positive Seebeck coefficient S value is an indication [3, 11, 21] of the hole mediated conduction in $Ca_3Co_4O_9$. The S values (Fig. 5) does not seem strongly to depend on the microstructure, with similar behaviours whatever the sintering process. For all samples S increases with temperature and reaches 180 μV/K at 873 K for CS. Such values are comparable to literature data [22, 27].

The temperature dependence of the thermoelectric power factor S^2/ρ, for the CS and SPS samples was deduced from the ρ and Seebeck coefficient S. At room temperature the power factor values of 88 and 260 $\mu W.m^{-1}.K^{-2}$ were obtained for the CS and SPS (1123 K) samples respectively. These values increase with the temperature up to 143 and 422 $\mu W.m^{-1}.K^{-2}$ at 873 K respectively. The SPS/1023K sample exhibits an intermediate power factor of 242 and 375 $\mu W.m^{-1}.K^{-2}$ at room temperature and 873 K respectively. The three times larger value of the SPS sample is due to densification improvement and grain alignment, both decreasing the resistivity. The power factor values obtained for the SPS can be compared with the best reported [22, 27] values of the literature.

4 Conclusions and outlook

Preformed $Ca_3Co_4O_9$ thermoelectric ceramics were free deformed and textured using Spark Plasma Sintering technique. The SPS technique allows the elaboration of highly dense materials (98%) with uniform grain morphology at lower temperature and shorter sintering times. Compared with the CS, the SPS sample exhibits a strong platelet orientation as evidenced by microstructure and texture analysis. High bulk density, lower electrical resistivity and improved of the thermoelectric power factor have been obtained. Finally, the SPS process is effective for enhancing of thermoelectric properties. The optimisation of other parameters as the maximum temperature, the holding time, and the uniaxial pressure applied during processing are under investigation.

Acknowledgments MP acknowledges a fellowship from the French Ministry of Research and Technology. The authors would like to acknowledge the financial support of "Conseil Régional de Basse-Normandie, France" for participation in the X-ray texture instrument financing.

References

1. I. Terasaki, Y. Sasago, K. Uchinokura, Phys. Rev. B. **56**, R12685–R12687 (1997)
2. M. Hervieu, Ph. Boullay, C. Michel, A. Maignan, B. Raveau, J. Solid. State. Chem. **142**, 305–318 (1999)
3. A.C. Masset, C. Michel, A. Maignan, M. Hervieu, O. Toulemonde, F. Studer, B. Raveau, J. Hejtmanek, Phys. Rev. B. **62**, 166–175 (2000)
4. M. Hervieu, A. Maignan, C. Michel, V. Hardy, N. Creon, B. Raveau, Phys.Rev. B. **67**, 045112–9 (2003)
5. A. Maignan, S. Hebert, L. Pi, D. Pelloquin, C. Martin, C. Michel, M. Hervieu, B. Raveau, Crys. Eng. **5**, 365–382 (2002)
6. T. Yamamoto, I. Tsukada, K. Uchinokura, M. Takagi, T. Tsubone, M. Ichihara, K. Kobayashi, Jpn. J. Appl. Phys. **39**, 747–750 (2000)
7. H. Muta, K. Kurosaki, S. Yamanaka, J. Alloys Compd. **350**, 292–295 (2003)
8. K. Kurosaki, T. Oyama, H. Muta, M. Uno, S. Yamanaka, J. Alloys Compd. **372**, 65–69 (2004)
9. A. Maignan, C. Martin, F. Damay, B. Raveau, J. Hejtmanek, Phys. Rev. B. **58**, 2758–2763 (1998)
10. G. Xu, R. Funahashi, Q. Pu, B. Liu, R. Tao, G. Wang, Z. Ding, Sol. State Ion. **171**, 147–151 (2004)
11. M . Prevel, O. Perez, J.G. Noudem, Sol. State Sci. **9**, 231–235 (2007)
12. M. Kazeoka, H. Hiramatsu, W.-S. Seo, K. Koumoto, J. Mater. Res. **13**, 523–526 (1998)
13. E.S. Reddy, J.G. Noudem, S. Hebert, C. Goupil, J. Phys. D: Appl. Phys. **38**, 3751–3755 (2005)
14. K. Ikoma, M. Munekiyo, K. Furuya, M. Kobayashi, T. Izumi, K. Shinohara, Thermoelectric module and generator for gasoline engine vehicles. Thermoelectrics, 1998. Proceedings ICT 98. XVII International Conference. pp 464–467 (1998), DOI 10.1109/ICT.1998.740419
15. R. Funahashi, S. Urata, K. Mizuno, T. Kouuchi, M. Mikami, Appl. Phys. Lett. **85**, 1036–1038 (2004)
16. R. Funahashi, M. Mikami, T. Mihara, S. Urata, N. Ando, J. Appl. Phys. **99**, 66117–66119 (2006)
17. M.E. Melo Jorge, A. Carreia dos Santos, M.R. Nunes, Int. J. Inorg. Mat. **3**, 915–921 (2001)
18. E. Guilmeau, R. Funahashi, M. Mikami, K. Chong, D. Chateigner, Appl. Phy. Lett. **85**, 1490–1492 (2004)
19. E. Guilmeau, H. Itahara, T. Tani, D. Chateigner, D. Grebille, J. Appl. Phys. **97**, 064902–1–064902-7 (2005)
20. Y. Masuda, D. Nagahama, H. Itahara, T. Tani, W.S. Seo, K. Koumoto, J. Mater. Chem. **13**, 1094–1099 (2003)
21. M. Prevel, S. Lemonnier, Y. Klein, S. Hébert, D. Chateigner, B. Ouladdiaf, J.G. Noudem, J. Appl. Phys. **98**, 93706–93709 (2005)
22. S. Horii, I. Matsubara, M. Sano, K. Fujie, M. Suzuki, R. Funahashi, M. Shikano, W. Shin, N. Murayama, J.-I. Shimoyama, K. Kishio, Jpn. J. Appl. Phys. **42**, 7018–7022 (2003)
23. M. Tokita, Mat. Sci. For. **492/493**, 711–718 (2005)
24. M. Yue, J.X. Zhang, W.Q. Liu, G.P. Wang, J. Magn. Magn. Mater. **271**, 364–368 (2004)
25. M. Suganuma, Y. Kitagawa, S. Wada, N. Murayama, J. Am. Ceram. Soc. **86**, 387–394 (2003)
26. J.X. Zhang, Q.M. Lu, K.G. Liu, L. Zhang, M.L. Zhou, Mat. Lett. **58**, 1981–4 (2004)
27. Y. Liu, Y. Lin, Z. Shi, C.-W. Nan, Z. Shen, J. Am. Ceram. Soc. **88**, 1337–1340 (2005)
28. K. Inoue, US Patent n° 3 250 892 (1966)
29. J. Ricote, D. Chateigner, Quantitative texture analysis applied to the study of preferential orientations in ferroelectric thin films Bol. Soc. Esp. Ceram. Vidrio. **38**(6), 587–591 (1999)

30. D. Chateigner (ed.), Combined analysis: structure-texture-microstructure-phase-stresses-reflectivity analysis by X-ray and neutron scattering, 147 pp (2004). http://www.ecole.ensicaen.fr/~chateign/texture/combined.pdf
31. S. Matthies, H.-R. Wenk, *Textures of Materials*, vol. 2, ed. by J.A. Szpunar (NRC Research, Ottawa, 1999), p. 1599
32. H.M. Rietveld, J. Appl. Cryst. **2**, 65 (1969)
33. S. Matthies, G.W. Vinel, Physica Status Solidi B. **112**, 111 (1982)
34. D. Chateigner, P. Germi, M. Pernet, J. Appl. Crystal. **25**, 766–769 (1992)
35. M. Mikami, E. Guilmeau, R. Funahashi, K. Chong, D. Chateigner, J. Mat. Res. **20**(9), 2491–2497 (2005)